Laser-Induced Crystallization of Standard Proteins on Ultra-Hydrophobic Surface and Characterization Using Raman Spectroscopy

B. Sudarshan Acharya, Sajan D. George, and Abdul Ajees Abdul Salam*
Department of Atomic and Molecular Physics, Manipal Academy of Higher Education, Manipal 576104, Karnataka, India

***e-mail:** abdul.ajees@manipal.edu

Abstract. Structural information helps to understand the function of the proteins and provides potential protein-ligand interactions of new drugs. X-ray crystallography is a powerful technique to determine the structure in three-dimensional geometry. However, obtaining high-quality single crystals remains an obstacle in macromolecular crystallography. Laser-induced crystallization is emerging as an alternative technique to circumvent this problem. In this study, we have prepared ultra-hydrophobic surfaces and used them for protein crystallization. Three model proteins, lysozyme, ferritin, and proteinase K, with distinct hydrophobicity, were used for this study. The protein droplet placed on three surfaces (non-siliconized, siliconized, and candle soot films) is exposed to a diode laser (785 nm, 75 mW). Ultra-hydrophobic candle soot surfaced coverslips rapidly yielded the crystals in conventional and laser-exposed droplets. Proteinase K nucleated faster than the lysozyme/ferritin on candle soot coated surface, compared to the regular coverslips suggesting that ultra-hydrophobic surfaces assisted laser-induced crystallization will play an essential role in protein crystallization.

Keywords: protein crystallization; ultra-hydrophobic surfaces; laser-induced crystallization.

Paper #7785 received 25 Feb 2023; revised manuscript received 20 Jul 2023; accepted for publication 21 Jul 2023; published online 4 Sep 2023. doi: 10.18287/JBPE23.09.030312.

1 Introduction

Proteins are essential for cell functioning because they produce required elements like cytoskeletons, metabolic enzymes, and signal-transmitting factors. Determination of the three-dimensional (3D) structure of proteins is essential to know its function [1]. X-ray crystallography is a gold standard technique to determine the 3D structure of the protein [2]. Protein structure determination using X-ray crystallography involves the following steps: (i) designing of the desired plasmid, (ii) cloning and expression of plasmids, (iii) large-scale purification of desired proteins, (iv) crystallization and optimization of purified proteins, (v) collecting X-ray diffraction data and refining the structure, and (vi) analyzing the 3D structure and predicting the function of the particular protein [3, 4]. However, the success of an X-ray diffraction technique purely depends on the quality of the single crystal [2]. Except for crystallization, other steps involved in protein structure determination through X-ray crystallography are a bit easier due to highly improved modern technologies [5]. Producing high-quality crystals of the preferable size is tedious, time-consuming, and the primary bottleneck. Nucleation and crystal growth are two steps in crystallization [6]. Nucleation is the first step of the crystallization process, which decides the property of the end product [5]. Thermodynamically, the proteins and small molecules will crystallize in the same fashion. In both cases, crystallization happens in a supersaturated state. In the case of small molecules, the supersaturation state is generally achieved by cooling the solvent from a higher temperature to room temperature. In the case of proteins,

This paper was presented at the International Conference on Nanoscience and Photonics for Medical Applications – ICNPMA, Manipal, India, December 28–30, 2022.

getting the protein into a supersaturation state and maintaining it in the same state is very difficult due to the precipitation problem. Vapor diffusion, batch crystallization, dialysis, and free interface diffusion are the conventional methods introduced to get protein into a supersaturated state [2, 5]. Various nucleation promoters known as nucleants and hydrophobic surfaces have been used to induce nucleation [7, 8]. These methods have little reproducibility probability due to the fragility and softness of protein crystals [1]. Laser-induced crystallization is an alternative and promising technique to crystallize small and biomolecules. Its advantages include accelerated growth of high-quality crystals, increased nucleation probability, broad applicability, polymorph selectivity, and spatiotemporal controllability [9].

In 1996, Garetz et al. reported the laser-induced crystallization of urea using a nanosecond laser of wavelength 1064 nm [10]. However, the limitation of the method is that it requires aged sample solutions and longtime laser exposure. The aging of the solution and longtime laser exposure is impropriating for biomolecules. Later several researchers used a femtosecond laser to crystallize different molecules, including proteins [11]. Unlike femtosecond lasers, a few molecules crystallized using the continuous-wave (CW) laser. Rungsimanon et al. reported the crystallization of glycine using a CW laser of wavelength 1064 nm and with a power of 1.1 W. In this case, the nucleation is due to an optical phenomenon known as laser trapping [12]. Caciagli et al. reported the laser-induced crystallization of colloids under the influence of the optofluidic force in the oil-water interface [13]. After that, several crystallization experiments are carried out using CW lasers [14–16].

In most cases, high-energy lasers, the pulsed laser beam from nanosecond to femtosecond duration, or several watts of CW lasers are used to induce nucleation. This is unsuitable in the case of the crystallization of biomolecules, especially proteins. Such factors may lead to the denaturation of biomolecules and/or structural disorders [6, 9, 17]. To overcome these problems, nucleants are introduced in laser-induced crystallization, known as photothermal laser-induced crystallization [9]. Recently our group crystallized lysozyme protein and all-natural amino acids using a novel technique called nucleate-assisted laser-induced crystallization [6, 9]. This study uses biocompatible materials such as coconut coir and peacock feathers as nucleants [6]. A combination of CW laser sources with biocompatible nucleants rapidly yielded the crystals (in seconds) with very low laser power (2–60 mW). In the current study, we present the effect of hydrophobic surfaces on the growth of three proteins using conventional and laser-induced crystallization methods.

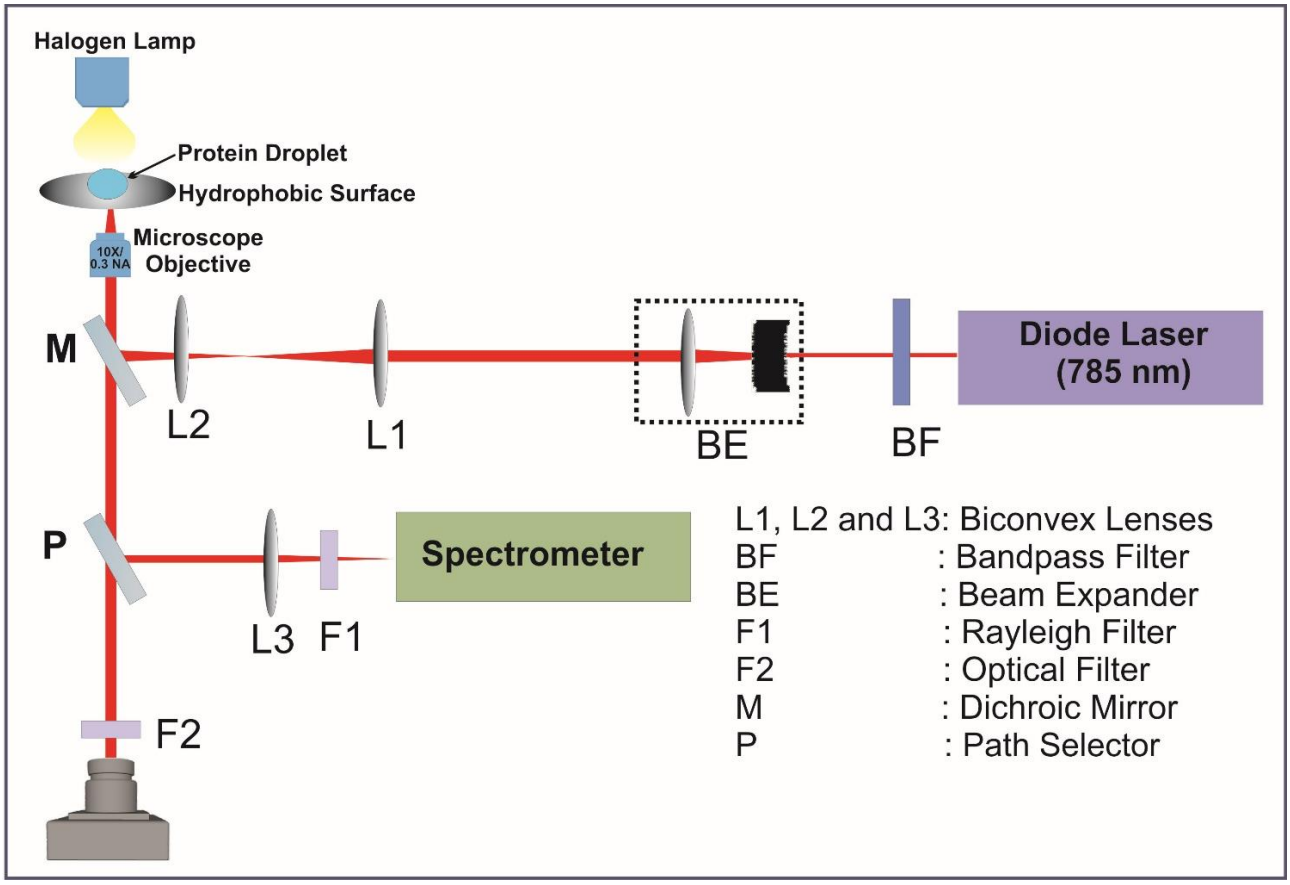

Fig. 1 A schematic diagram of the optical setup used for laser-induced crystallization and Raman spectroscopy is shown.

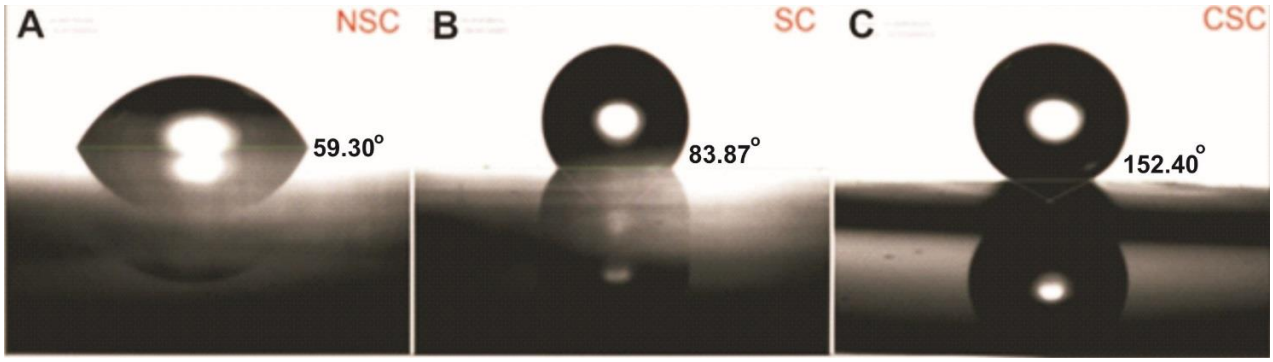

Fig. 2 Contact angle measurements of (A) NSC (59.30°), (B) SC (83.87°), and (C) CSC (152.4°), respectively.

Table 1 Proteins and chemicals selected for crystallization and time taken for crystallization.

Sl. No.	Protein	Protein solution	Well buffer	Time is taken for crystallization (in hours)					
				NSC		SC		CSC	
				Conventional	Laser	Conventional	Laser	Conventional	Laser
1	Lysozyme (Sigma #L-6876) 40 mg/ml	100 mM NaOAc (pH 4.8)	1 M NaCl, 0.1M NaOAc (pH 4.8)	18	4	12	4	12	6
2	Proteinase K (Sigma #P-2308) 20 mg/ml	25mM Tris (pH 7.5)	1.2 M $(NH_4)_2SO_4$, 0.1 M Sodium Cacodylate (pH 6.2)	12	6	12	6	6	2
3	Ferritin (Sigma #F4503) 20 mg/ml	Distilled water	0.8 M $(NH_4)_2SO_4$, 60 mM $CdSO_4$, and 0.1 M Tris (pH 7.5)	32	32	32	18	12	6

2 Materials and Methods

2.1 Chemical and Proteins

The analytical grade chemicals required for the study were purchased from SRL (India), Sigma Aldrich (USA), and Merck (USA). Non-siliconized coverslips were purchased from Blue Star (India) and siliconized coverslips from Hampton Research (USA) and used for protein crystallization without any modifications. Proteins for this study were obtained from Sigma Aldrich and used without further purification. The desired amount of protein samples is either dissolved by deionized water or suitable buffers based on the solubility, pH, and stability. The details of the buffer conditions for each protein are given in Table 1.

2.2 Synthesis of Ultra-hydrophobic Surface

Three types of 22 mm glass coverslips (Hampton Research, HR3-254), namely (1) non-siliconized (NSC), (2) siliconized (SC), and (3) candle soot film (CSC) was used for this crystallization study. Candle soot films (CSC) were prepared in four steps. In the first step, the 5 µl of polydimethylsiloxane (PDMS) solution was uniformly coated on coverslips using a spin coater. In the second step, these PDMS-coated coverslips were exposed to candle soot such that the candle soot flame covers the entire surface. The coverslips were incubated at 85 °C for 2 h in the third step. In the final stage, the dried coverslips were washed once using distilled water and incubated again at 85 °C for 15 min.

2.3 Contact Angle Measurement

To understand the hydrophobicity of the coverslips, the contact angle was measured with a 20 µl water droplet placed on NSC, SC, and CSC coverslips using a commercial contact angle meter (model: HO-IAD-CAM-01B, Halmarc, India). The experiment was repeated three times in each case, and the average of contact angles was calculated.

2.4 Crystallization

The hanging drop method was used to crystallize all the proteins using Linbro 24 well plates (HR3-110; Hampton Research, Aliso Viejo, CA). 5 µl volume of protein solutions was pipetted on the coverslips and mixed with an equal volume of well-buffers given in Table 1.

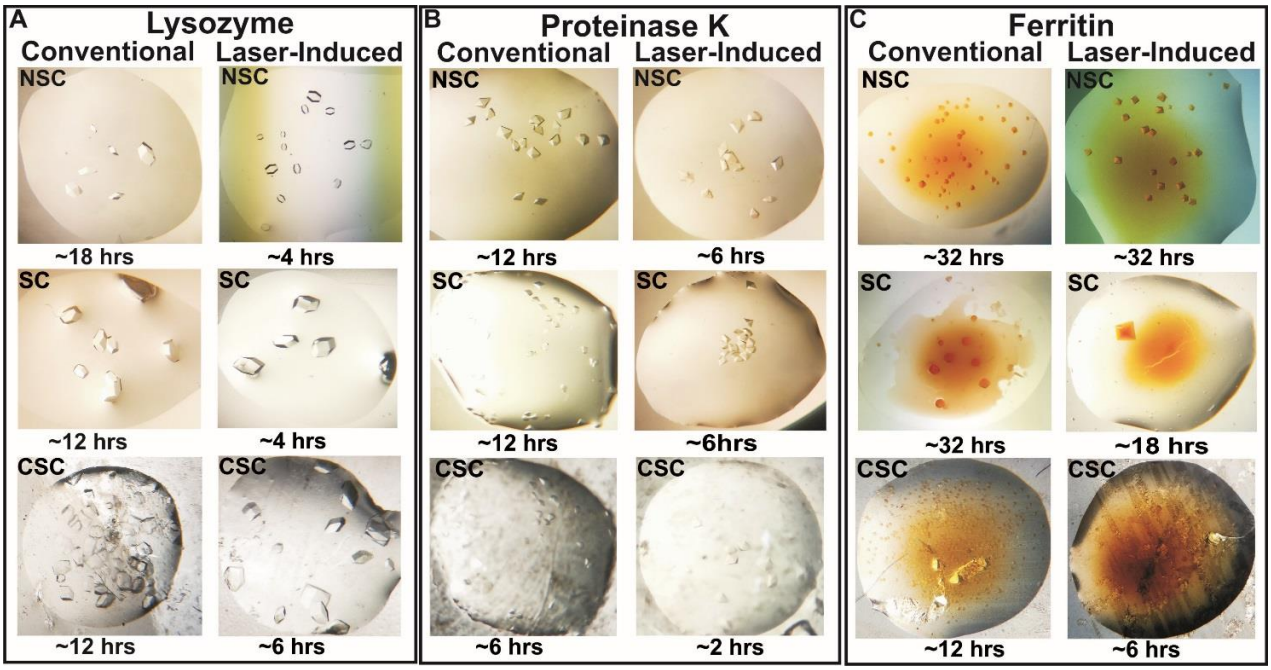

Fig. 3 Conventional and laser-induced crystallization results of the (A) lysozyme, (B) proteinase k, and (C) ferritin protein crystallized on three different surfaces.

Then the drops were subjected to the diode laser (Starbright Diode Laser, Torsana Laser Tech, Denmark) beam of wavelength 785 nm with 75 mW laser power for one minute. A microscope monitored laser-exposed mixtures to identify the protein crystals and eliminate the false positive crystals. After the laser exposure, the crystallization plates were placed at a constant temperate of 19 °C in a clean environment without disturbance. The plates were observed every 2 h for the initial 6 h. After that, the plates were followed every 6 h up to the initial 24 h and then every day for a few more days. Protein's physical and chemical properties were analyzed using the *ProtParam* online tool (https://web.expasy.org/cgi-bin/protparam/ protparam).

2.5 Optical Setup for Crystallization and Characterization

Crystallization of proteins and characterization were carried out by a micro-Raman arrangement built around a CW diode laser (785 nm wavelength, Starbright, Denmark) [6, 9]. The experimental setup used for crystallization is built around an inverted microscope, as shown in a schematic diagram (Fig. 1). The laser beam (~2 mm diameter) was expanded using manual beam expanders (BE) to a size of 9 mm.

A 1:1 telescopic arrangement and a dichroic mirror (M1) with high reflectivity at 785 nm were used to steer the expanded beam to the back aperture of a microscope objective (60X objective of 0.85 NA). A CCD camera (Nikon Eclipse Ti-U, Japan) captured images of grown crystals through an inverted microscope with a 10× objective of 0.3 NA under a halogen lamp. The protein crystals were characterized by Raman spectroscopy. Raman signals were measured (60× objective of 0.85 NA) by a spectrometer (Horiba Jobin Yvon iHR320) coupled with a liquid-nitrogen-cooled CCD detector (Symphony CCD-1024×256-OPEN-1LS). In all our experiments, Raman spectra of protein crystals were recorded at a constant laser power of 12 mW using 60 s integration time as described [6, 9].

3 Results and Discussion

3.1 Contact Angles of Three Different Surfaces

The contact angles for NSC, SC, and CSC are 59.30º, 83.87º, and 152.4º, respectively. It suggests that the CSC is ultra-hydrophobic compared to the other two surfaces because the contact angle of the candle soot films is greater than 150º (Fig. 2).

3.2 Crystallization of Proteins on the Ultra-Hydrophobic Surface

The proteins lysozyme, proteinase K, and ferritin were initially crystallized in the conventional protein crystallization method using the hanging drop method. The results are shown in Table 1 and Fig. 3. In the conventional method, the lysozyme crystals were observed on SC and CSC after 12 h and 18 h on NSC. The proteinase K crystals were observed at 12 h on NSC and SC coverslips and 6 h in CSC coverslips. The ferritin crystals took 32 h to grow on NSC and SC coverslips and 12 h on CSC. Later the protein crystallization experiments were repeated using the laser-induced crystallization method, and the results are summarized in Table 1 and Fig. 3. In the case of lysozyme, the formation of the crystals was observed in laser-induced droplets placed in NSC, SC within ~4 h and ~6 h in CSC coverslip.

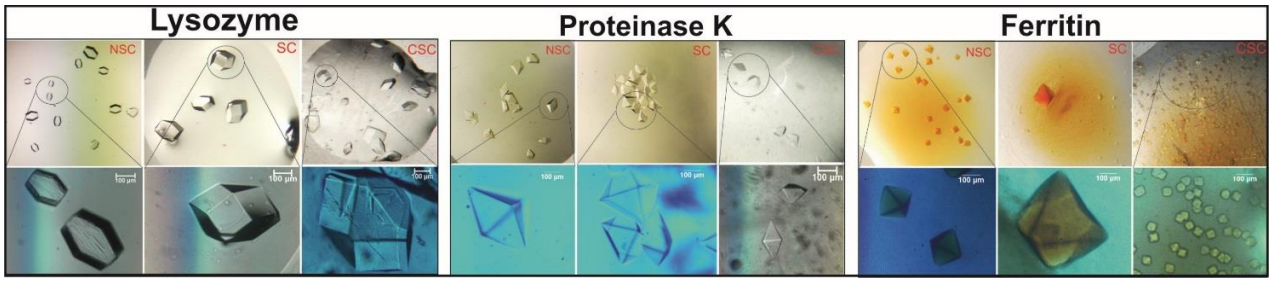

Fig. 4 Microscopic view of protein crystals crystallized on three different surfaces by laser-induced crystallization.

Table 2 Raman bands and assignments for single lysozyme crystal in the spectral region of 500–1800 cm^{-1}.

Band frequency (cm^{-1})	Assignments	Band frequency (cm^{-1})	Assignments
506	ν(S–S) ggg	#1258	amide III (random coil)
528	ν(S–S) ggt	#1289	amide III (α-Helix)
573	Tryptophan	*1292	amide III (α-Helix)
643	Tyrosine	1312	δ(CH_2)
694	Methionine ν(C–S)	1336	Tryptophan (Fermi doublet)
723	Cysteine ν(C–S)	1358	Tryptophan (Fermi doublet)
759	Tryptophan (W18 mode)	1386	Cα-H bending
833	Tyrosine (Fermi doublet)	1389	Proline
855	Tyrosine (Fermi doublet)	1407	Histidine
872	Tryptophan	1423	Tryptophan
896	Main chain vibration ν(Cα–C)	1442	Glycine
929	Main chain vibration ν(Cα–C)	1444	CH deformational vibrations
1003	Phenylalanine (F1 mode)	1456	CH deformational vibrations
1025	Phenylalanine	1467	δ(CH_2)
1048	ν(C–N)	1486	Tryptophan
1072	ν(C–N)	1513	amide II
1102	Proline, Alanine, σ(Cα–N), σ(C–C)	1549	δ(CH_3)
1127	Tryptophan σ(C–C), σ(C–N)	1576	Phenylalanine
1154	δ(CH_3)	1602	Phenylalanine (ring mode)
1175	Tyrosine, δ(CH_3)	1613	Tyrosine
1208	Tyrosine, Phenylalanine, Tryptophan	1615	Tyrosine, Tryptophan
#1231	amide III (β-sheet)	1654	amide I (α-helix)
*1242	amide III (β-sheet)		

The band frequencies marked with * correspond to the lysozyme crystal grown on NSC by the conventional method, and the frequencies marked with # correspond to the crystals grown on SC and CSC.

Laser-induced crystals of proteinase K were observed in NCS and SC within ~6 h and CSC within ~2 h. The ferritin crystals took a similar time (~32 h) to grow on NSC surfaces for conventional and laser-induced methods. However, the SC (~18 h) and CSC (~6 h) surfaces yielded the ferritin crystals faster in the laser-induced method than in the conventional method. In addition, the crystal size of all three proteins is significantly bigger in the laser-induced method droplets compared to the conventional method in most of the cases (Fig. 4).

3.3 Structural Studies Using Raman Spectroscopy

Raman spectrum of three proteins were recorded in the range of 500–1850 cm^{-1} for the analysis, called as fingerprint region of the protein [18, 19]. Analysis of this region will provide information about the vibrations of aromatic amino-acid residues, disulfide bonds, protein secondary structure dynamics based on amide I and

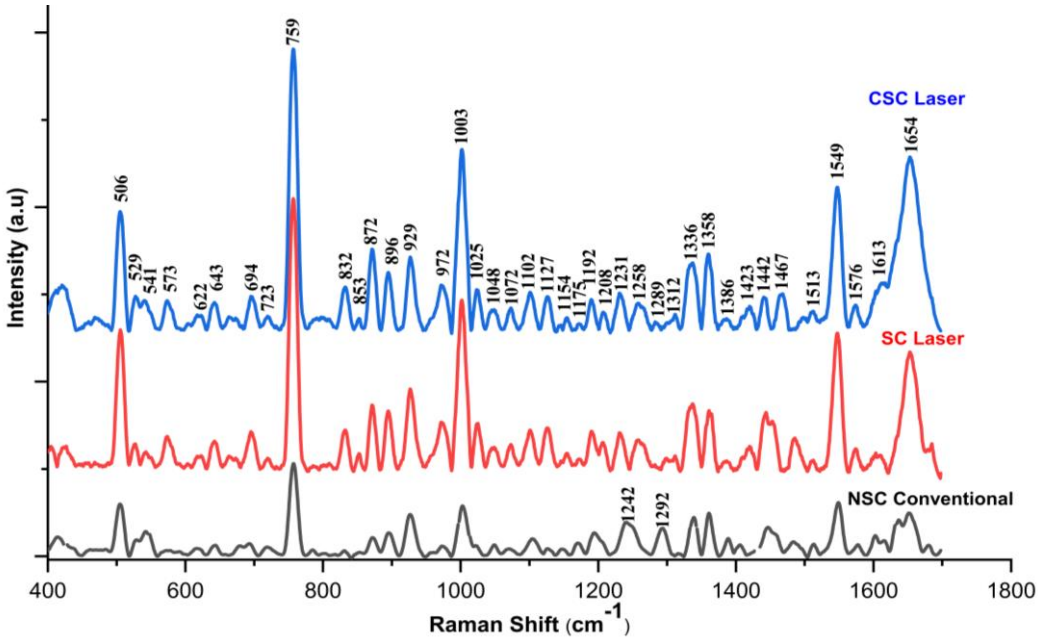

Fig. 5 Raman spectra of lysozyme crystals grown on the NSC surface using the conventional method and those grown on SC and CSC using the laser-induced method.

amide III bands, and modes related to polypeptide backbone [20]. Knowing the positions of the amide I and amide III bands helps interpret the dynamics of protein secondary structure [9, 18]. Raman spectra can be used to characterize the secondary structure conformation changes of proteins [9, 21]. We have used Raman spectroscopy to confirm the structural modifications of the proteins taken for this study.

In order to verify whether the laser source and/or the three surfaces used to grow the crystals caused any structural changes in any of these three proteins, Raman spectra of lysozyme, proteinase K, and ferritin protein crystals grown on non-siliconized coverslip (NSC) using the conventional crystallization method the protein crystals grown on siliconized coverslip (SC), and candle soot film (CSC) surfaces using laser-induced crystallization method were recorded. The frequency assignments for Raman spectra of lysozyme, proteinase k, and ferritin crystals are summarized in Tables 2–4, respectively. In lysozyme protein, around 40 peaks were measured for each case (Table 2), and detailed molecular vibrations were assigned for all the peaks. The signature five major peaks (506 cm^{-1}, 759 cm^{-1}, 1003 cm^{-1}, 1506 cm^{-1}, and 1654 cm^{-1}) and tryptophan doublet (1336 cm^{-1} and 1358 cm^{-1}) are observed for all three lysozyme crystals. The Raman spectra recorded for lysozyme crystals grown using the conventional crystallization method on the NSC surface, and the Raman spectra recorded for lysozyme crystals grown on SC, and CSC surfaces using the laser-induced crystallization method are similar. A few minor differences are observed for crystals grown on NSC and SC surfaces in comparison with the crystals grown on CSC surfaces. For example, the lysozyme crystals grown on the NSC surface using the conventional method showed two additional minor peaks (1242 cm^{-1} and 1292 $cm^{-1)}$. Similarly, three minor peaks (1231 cm^{-1}, 1258 cm^{-1}, and 1289 $cm^{-1)}$ are observed for crystals grown using laser-induced crystallization methods on SC and CSC surfaces, and these peaks correspond to amide III bands. The Raman spectrum of lysozyme proteins such as the amide I (1600–1700 cm^{-1}), amide III (1220–1300 cm^{-1}), C–C stretches (901–960 cm^{-1}), and disulfide (500–550 cm^{-1}) reported by the previous reports are matching with the current study [18, 20, 22]. The Raman spectrum of proteinase K protein yields 26 peaks with a major peak at 976 cm^{-1}, which belongs to the tryptophan vibration mode. All three proteinase K Raman spectra recorded for the crystals grown under conventional (NSC) and laser-induced (SC and CSC) methods showed similar range, and there are no major or minor differences are noted (Table 3). Similarly, the Raman spectrum recorded for the ferritin crystals yielded 28 peaks for those grown under NSC, SC, and CSC conditions. Once again, the ferritin crystal also showed a major peak at 976 cm^{-1} (Table 4).

4 Discussion

4.1 Crystallization

4.1.1 Effect of Hydrophobic Surfaces

Protein crystallization and 3D structure determination play a crucial role in various fields, including drug design, drug formulations, drug delivery, the pharmaceutical industry, biomaterial manufacture, food packaging, food delivery, and structural biology [6]. The protein crystallization process can be controlled by surface modification due to the hydrophobic interactions of proteins. The air/solution, oil/solution, microfluidic, and nanoparticle interfaces are studies conducted for several

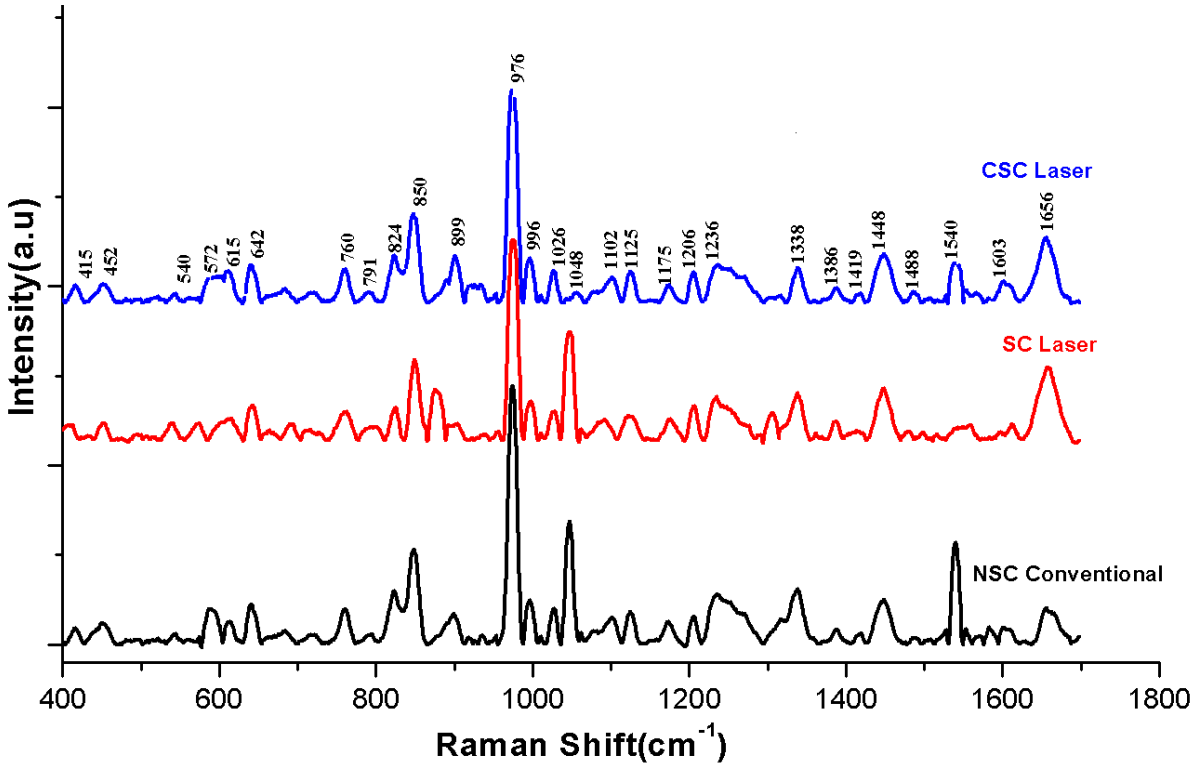

Fig. 6 Raman spectra of proteinase k crystals grown on the NSC surface using the conventional method and those grown on SC and CSC using the laser-induced method.

Table 3 Raman bands and assignments for proteinase k single crystal in the spectral region of 500–1800 cm^{-1}.

Band frequency (cm^{-1})	Assignments	Band frequency (cm^{-1})	Assignments
540	ν(S–S)	1102	Proline, Alanine, σ(Cα–N), σ(C–C) (stretching)
572	Tryptophan/Cytosine, Guanine	1125	Tryptophan σ(C–C), σ(C–N)
615	C–C twisting of protein	1175	Tyrosine, δ(CH_3)
642	Tyrosine	1206	Phenylalanine
760	Tryptophan, δ(ring)	1236	amide III (β- sheet)
791	Pyrimidine	1338	Tryptophan
824	Tyrosine (Fermi doublet)	1386	Cα-H bending
850	Tyrosine (Fermi doublet)	1419	δ(CH_2) aliphatic side chains
876	ν(C–C), hydroxyproline	1448	C–H (deformation)
976	Tryptophan	1488	Phenylalanine/Guanine (N7)
996	Phenylalanine	1540	amide II (N–H bending vibration)
1026	Phenylalanine	1603	Phenylalanine (ring mode)
1048	Phenylalanine, ν(C–N)	1656	amide I (α-helix)

proteins and proved effective in controlling protein nucleation [23–27]. Siliconized coverslips coated with poly-L-lysine and hexamethyl-D-disilane are used to grow the lysozyme crystals to understand the thermodynamics of homogenous and heterogeneous nucleation processes [28]. Lysozyme protein is coated on the coverslips and used as a thin film to grow the protein crystals, yielding bigger protein crystals than the conventional hanging drop method [29]. Surface modification by adding various nucleants is another popular method routinely used to accelerate protein growth [6, 9, 30, 31]. Surface modification-based crystallization has several advantages; (i) increasing possibilities to get desired crystal sizes, shapes, and forms without changing the buffer conditions, pH, and temperature, (ii) significantly reducing the nucleation time, (iii) obtaining the protein crystals at very low supersaturation level and optimization, (iv) expedite the overall crystallization process, and (v) cost reduction to develop new pharmaceutical products [32]. The current work uses the simple and cost-effective CSC surface modification technique, showing several advantages.

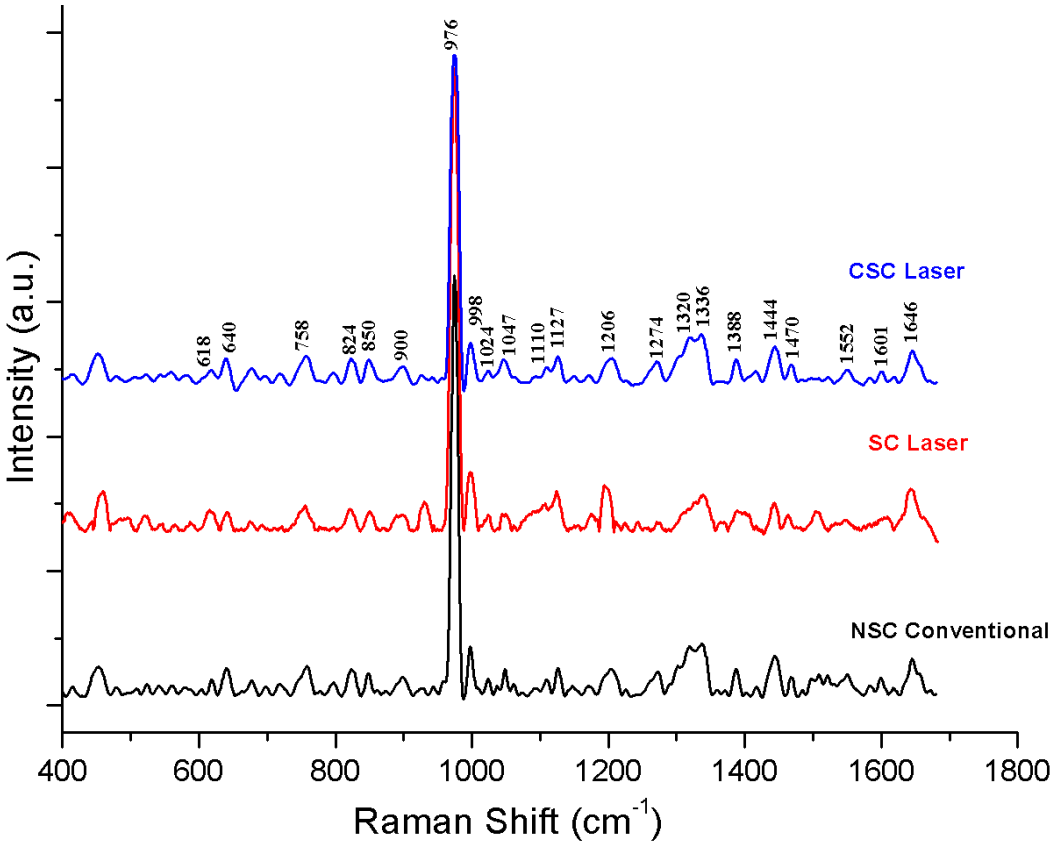

Fig.7 Raman spectra of ferritin crystals grown on the NSC surface using the conventional method and those grown on SC and CSC using the laser-induced method.

Table 4 Raman bands and assignments for ferritin single crystal in the spectral region of 500–1800 cm^{-1}.

Band frequency (cm^{-1})	Assignments	Band frequency (cm^{-1})	Assignments
521	S–S disulfide stretching	1127	ν(C–N)
619	C–C twisting	1197	Tryptophan ring breathing
640	C–S stretching & C–C twisting	1206	Hydroxy-proline, tyrosine
758	Tryptophan	1274	amide III (α-helix)
824	Tyrosine (Fermi doublet)	1320	CH deformation
850	Tyrosine (Fermi doublet)	1336	δ(CH_3) δ(CH_2) twisting
896	Tryptophan	1388	CH_3 band
900	C–C stretching vibration	1444	CH_2 deformation
932	Skeletal C–C, α-helix	1470	C=N stretching
976	Tryptophan	1548	amide II, Tryptophan
998	ν(C–C)	1552	Tryptophan
1024	ν(C–N)	1601	amide I (C=O stretching)
1047	ν(C–N)	1608	Tyrosine, Tryptophan, Phenylalanine
1110	C–C and C–N stretching	1646	amide I (α-helix)

The CSC surface generally yielded the protein crystals faster than the NSC and SC surfaces (Table 1 and Fig. 3). For example, proteinase K crystals were observed ~12 h on the NSC surface, whereas the time is reduced to 6 h on the CSC surface. The CSC surface under the laser-induced crystallization method yielded crystals faster than NSC and SC surfaces. Almost 50% time reduction is observed for all three protein crystals grown on the CSC surface using a laser-induced crystallization technique. The nucleation time is reduced to half when the hydrophobicity of the coverslip is increased. A similar trend is also observed for ferritin.

In addition, proteins' hydrophobic or hydrophilic nature shows some interesting results. Lysozyme comprises 129 amino acids with a molecular weight of 14.3 kDa. The theoretical pI is 9.32, and the

hydropathicity (GRAVY) is −0.472. The proteinase K contains 279 amino acids (molecular weight 28.9 kD), the theoretical pI is 7.80, and the hydropathicity (GRAVY) is −0.228. The ferritin is ~20 kDa protein comprised of 165 amino acids with a theoretical pI of 9.76, and the hydropathicity (GRAVY) is −0.378. The increasing positive value of grant average hydropathicity (GRAVY) indicates a greater hydrophobicity. The proteinase K is poorly water-soluble than lysozyme. water-soluble than lysozyme.

It should be noted that proteinase K crystallized faster in CSC coverslips than the other two proteins. This indicates that proteinase K can be crystallized faster on the CSC surfaces. Lysozyme has a hydrophilic surface and prefers to crystallize on hydrophilic surfaces. Thus, the results suggest that surface chemistry certainly plays an essential role in the crystallization of proteins and may influence nucleation.

4.1.2 Effect of Laser on Crystal Growth

Laser-induced crystallization method is an emerging alternative technique for growing small and macromolecule crystals. We have produced various small molecules (NaCl, KCl, chalcone compounds, and amino acids) and proteins (lysozyme) using CW and ultrafast laser sources [6, 9]. In the current study, we are interested in studying the effect of hydrophobic surfaces on protein crystal growth using conventional and laser-induced crystallization techniques. The study was conducted for their proteins, namely lysozyme, ferritin, and proteinase K using conventional and laser-induced crystallization methods in three different hydrophobic surfaces NSC, SC, and CSC. The results suggest that in general, the laser-induced crystallization method helps to obtain the crystals faster on all three surfaces, except ferritin under NSC. The ferritin crystals took ~32 h to grow on NSC surfaces for conventional and laser-induced methods. Thus, the results showed that in terms of crystal growth time, the laser-induced crystallization method did not show any advantage on the ferritin crystals growth on the NSC surface. At the same time, the same ferritin protein crystals were grown in ~18 h under the laser-induced method on the SC surface, which is ~1.8 times faster than the crystals grown using the conventional method (Table 1 and Fig. 3C). Similarly, the crystals grown on CSC surfaces on both conventional and laser-induced crystallization methods yielded the crystals faster. The ferritin crystals were grown on the CSC surface within 6 h under the laser-induced crystallization method, which is ~5.3 faster than the crystals grown on NSC surfaces. A similar trend is observed for proteinase K crystals grown in NSC and SC surfaces. However, the proteinase K crystals have grown much faster than lysozyme and ferritin on the CSC surface within ~2 h. Apart from the time reduction, the laser-induced method reduced the nucleation sites. Due to this effect, the crystals are bigger than those in the conventional method (Fig. 5). This phenomenon was observed and reported [6, 9, 11]. In the case of ferritin, a large number of small crystals were observed with few bigger crystals on CSC. This shows a high nucleation probability (Fig. 4). Compared with the conventional the laser-induced crystallization technique yielded the crystals faster in all three cases, and crystals grown on SC and CSC are highly diffractive [6, 7].

We notice that the probability of finding crystals on the focal region of the laser is maximum in most cases (Figs. 3 and 4). In the case of proteinase k, the protein crystals are concentrated at the focal area. In the case of ferritin, we observed only one single crystal growth with a large size. The CSCs are ultra-hydrophobic and highly biocompatible, with higher contact angle values than the other two surfaces [33]. In general, we observed that the crystal growth rate is high on CSC in conventional and laser-induced crystallization techniques. This is mainly due to the porous nature of the material [33, 34]. There is an increase in the solute concentration due to the trapping of solute molecules inside the pores, and pore walls provide free energy, which drives the adsorption of solute molecules. Due to this, a supersaturated state will form at pores, which leads to nucleation [35, 36]. So, these pores present on the surface will act as nucleation sites.

4.2 Raman Spectroscopic Studies

Raman spectroscopy is used to validate the structural properties of the protein [37]. Compared with the solution, protein crystals have a narrower Raman band with less peak broadening [38]. Generally, in solution, the molecules are subject to constant movement and frequent intermolecular collisions [37]. The vibrational modes are used to analyze the protein structures. The CONH group of proteins, which forms the peptide bond, is associated with nine vibrational modes. The amide I band ranges from 1600 cm^{-1} to 1700 cm^{-1} helps study the proteins' C=O (~80%) and C–N (~20%) stretching contributions. The amide II band ranges from 1480 cm^{-1} to 1580 cm^{-1} is helpful in the study of the out-of-phase combination of the NH bending and CN stretching vibrations. The amide III band ranges from 1220 cm^{-1} to 1400 cm^{-1} in-phase combination of the NH bending and CN stretching vibrations. It should be noted that the side chain conformational changes of the proteins can be analyzed using intensity changes of amide III bands [39]. The amide II bands are very sensitive to the backbone conformational changes of the proteins. Hence secondary structural information such as α-helix (1300 cm^{-1}), β-sheet, and random coil (1240 cm^{-1}) can be analyzed using amide III bands. Amide IV (625−770 cm^{-1}), amide V (640−800 cm^{-1}), and amide VI (540−600 cm^{-1}) are helpful to study the conformational changes of OCN bending, out-of-plane CN bending, and out-of-plane C=O bending. The structural analysis of the proteins is mainly studied using amide I, II, and III bands.

The amide I band appears mainly due to C=O stretching vibrations, and in addition, there is the contribution from N–H bending, C–N stretching, and C–C–N deformations [20, 21]. Amide I peak in Raman spectra indicates the strength of hydrogen bonds formed by dipole-dipole interactions between C=O and N–H groups of amides [20]. In the Raman spectra recorded for

all three lysozyme crystals (Fig. 5), the amide I band from α-helix appeared at 1654 cm^{-1}, which matches well with the literature [18, 20]. Similarly, the amide I band for proteinase k and ferritin crystals (Fig. 6) appeared at 1656 cm^{-1} (α-helix) and 1646 cm^{-1} (α-helix) (Fig. 7), respectively [19]. For the disordered protein structures, the amide I band occurs at a higher wavenumber region of 1680–1695 cm^{-1} [9, 19, 22]. This implies that the 3D structure of all three proteins taken for this study is unaltered by laser or CSC.

The amide II bands are observed at 1513 cm^{-1} for lysozyme, at 1540 cm^{-1} for proteinase k, and at 1548 cm^{-1} ferritin crystals and are well supported by the literature [20, 40, 41]. Similarly, the amide-III bands at 1231 cm^{-1} (β-sheet) and 1258 cm^{-1} (random coil) are observed for lysozyme crystals. In addition, two minor peaks at 1242 cm^{-1} (β-sheet) and 1292 cm^{-1} (α-helix) are observed for the lysozyme crystals grown on NSC coverslips using conventional crystallization methods. A similar observation is also found in the literature for lysozyme protein [21, 42, 43]. For proteinase K the amide III bands are observed at 1236 cm^{-1} (β-sheet), and in the case of ferritin at 1274 cm^{-1} (α-helix), similar observations have already been reported [19]. Thus, as we discussed earlier amide III bands are very sensitive to protein backbone conformation. The protein profiles recorded for all three proteins match the literature, thus confirming that the protein structures are not undergoing conformational changes.

In all three proteins, the tryptophan peaks showed the highest intensity at 759 cm^{-1} for lysozyme and 976 cm^{-1} for the other two proteins. Lysozyme has a peak at 1003 cm^{-1}, which corresponds to the F1 mode of phenylalanine and is well supported by the literature [20, 41]. The peak observed around 872 cm^{-1} is a signature lysozyme peak known as the W17 mode of tryptophan. W17 mode is an important marker for forming a strong hydrogen bond of the tryptophan-28 indole ring, which matches the literature [21]. The lysozyme protein has six tryptophan residues. Four of them are solvent exposed and situated on the outer surface of the lysozyme. The W17 mode indicates that tryptophan residues of lysozyme are involved in a very strong hydrogen bonding [9].

Lysozyme protein has four disulfide bridges. The peak at 506 cm^{-1} (ggg confirmation) and 528 cm^{-1} (ggt confirmation) correspond to vibrations of disulfide bonds between cysteine residues of lysozyme [18, 20]. Cys34-Cys123 and Cysl78-Cys249 are the two disulfide bonds of the proteinase k, and the Raman peak at 540 cm^{-1} (Fig. 7) corresponds to the vibrations of disulfide bonds of proteinase k [41, 44]. In the case of ferritin, S–S disulfide stretching is observed at 521 cm^{-1} and confirmed by the literature [41]. Rygula et al. reported that the band related to the stretching vibration of disulfide bonds is not observed for ferritin due to the absence of disulfide bridges in the protein [19]. In the current study, we have prepared the ferritin solution using distilled water, and there is a high possibility that the due to oxidation of cysteine residues the disulfide bonds appeared [45–47].

5 Conclusion

In macromolecular X-ray crystallography, except crystallization, all other steps are automated. Most challenges are solved using advances in experimental techniques and artificial intelligence-enabled high-end computational systems. Obtaining large enough crystals, which helps to collect high-resolution diffraction data, and subsequent atomic resolution 3D structures from protein crystals are still considered to be one of the bottlenecks in structural biology. Optimizing several crystallization variable parameters such as temperature, pH, buffer conditions, salts, ions, additives, and detergents makes the crystallization process challenging. Most of the time, the available amount of protein is also limited, restricting the number of crystallization trials. To overcome these issues, the high-throughput crystallization process involving data collection using micron-sized protein crystals through synchrotron sources, X-ray free-electron lasers, data collection techniques like serial synchrotron crystallography, and serial femtosecond crystallography have been successfully utilized. However, developing suitable protein crystals for these studies is still inevitable. In this work, we have crystallized the lysozyme, proteinase K, and ferritin proteins in three different surfaces: NSC, SC, and CSC, using conventional and laser-induced (CW 785 nm laser) crystallization methods. We have produced the protein crystals faster and bigger using ultra-hydrophobic coverslips made up of CSC. We have proved that the protein crystals in CSC can be grown more quickly than NSC and SC coverslips. For all three proteins, both conventional and laser-induced methods, the hydrophobic CSC surface yielded the crystals faster.

The CSC coverslips are easy to prepare and cost-effective. The hydrophobicity of the CSC surfaces can be easily customized based on the protein's hydrophobic properties. In addition, laser-induced crystallographic studies accelerate the crystallization process and help us to grow suitable diffraction-quality crystals in less than 24 h. Proteinase K yielded the crystals within 2 h, and lysozyme and ferritin took 6 h. The Raman spectroscopy results unambiguously proved that neither the CSC nor laser sources do not alter the protein structure. Thus, the current proposed study might be beneficial for obtaining the protein crystals rapidly. The study can be extended to more proteins, especially membrane proteins which are difficult to purify and crystallize.

6 Acknowledgment

Abdul Ajees Abdul Salam acknowledges the research grant provided by the Manipal Academy of Higher Education (MAHE) under intramural funding (MAHE/DREG/PhD/IMF/2019).

Disclosures

The authors declare no conflict of interest.

References

1. M. Kashii, H. Kitano, Y. Hosokawa, H. Adachi, Y. Mori, T. Sasaki, H. Masuhara, K. Takano, H. Matsumura, and T. Inoue, "Femtosecond laser processing of protein crystals in crystallization drop," Japanese Journal of Applied Physics 44(6L), L873 (2005).
2. M. A. Dessau, Y. Modis, "Protein crystallization for X-ray crystallography," Journal of Visualized Experiments 47, e2285 (2011).
3. A. Moreno, "Advanced methods of protein crystallization," Protein Crystallography. Methods in Molecular Biology 1607, A. Wlodawer, Z. Dauter, M. Jaskolski (Eds.), Humana Press, New York (2017).
4. J. M. Keith (Ed.), "Data, sequence analysis and evolution. Preface," Methods in Molecular Biology 452, Totowa, NJ (2008).
5. A. McPherson, J. A. Gavira, "Introduction to protein crystallization," Acta Crystallographica Section F: Structural Biology Communications 70(1), 2–20 (2014).
6. S. Thippeshappa, S. D. George, A. Bankapur, S. Chidangil, D. Mathur, and A. A. A. Salam, "Effect of biocompatible nucleants in rapid crystallization of natural amino acids using a CW Nd:YAG laser," Scientific Reports 8, 16018 (2018).
7. C. N. Nanev, E. Saridakis, L. Govada, S. C. Kassen, H. V. Solomon, and N. E. Chayen, "Hydrophobic Interface-Assisted Protein Crystallization: Theory and Experiment," ACS Applied Materials & Interfaces 11(13), 12931–12940 (2019).
8. T. A. J. Grell, M. A. Pinard, D. Pettis, and K. Aslan, "Rapid crystallization of glycine using metal-assisted and microwave-accelerated evaporative crystallization: The effect of engineered surfaces and sample volume," Nano Biomedicine and Engineering 4(3), 125–131 (2012).
9. T. Shilpa, S. D. George, A. Bankapur, and S. Chidangil, A. K. Dharmadhikari, D. Mathur, S. M. Kumar, K. Byrappa, and A. A. A. Salam, "Effect of nucleants in photothermally assisted crystallization," Photochemical & Photobiological Sciences 16(6), 870–882 (2017).
10. B. A. Garetz, J. E. Aber, N. L. Goddard, R. G. Young, and A. S. Myerson, "Nonphotochemical, polarization-dependent, laser-induced nucleation in supersaturated aqueous urea solutions," Physical Review Letters 77(16), 3475–3476 (1996).
11. T. Shilpa, S. G. Bhat, V. R. Rodrigus, S. George, A. K. Dharmadhikari, C. Santhosh, and A. A. Ajees, "Small and macromolecules crystallization induced by focused ultrafast laser," Proceedings of the Indian National Science Academy 81(2), 517–523 (2015).
12. T. Rungsimanon, K. I. Yuyama, T. Sugiyama, and H. Masuhara, "Crystallization in unsaturated glycine/D2O solution achieved by irradiating a focused continuous wave near infrared laser," Crystal Growth & Design 10(11), 4686–4688 (2010).
13. A. Caciagli, R. Singh, D. Joshi, R. Adhikari, and E. Eiser, "Controlled Optofluidic Crystallization of Colloids Tethered at Interfaces," Physical Review Letters 125(6), 068001 (2020).
14. K. I. Yuyama, K.-D. Chang, J. R. Tu, H. Masuhara, and T. Sugiyama, "Rapid localized crystallization of lysozyme by laser trapping," Physical Chemistry Chemical Physics 20(9), 6034–6039 (2018).
15. J. R. Tu, A. Miura, K. I. Yuyama, H. Masuhara, and T. Sugiyama, "Crystal growth of lysozyme controlled by laser trapping," Crystal Growth & Design 14(1), 15–22 (2014).
16. J. J. K. Chen, K.-I. Yuyama, T. Sugiyama, and H. Masuhara, "Bubble generation and molecular crystallization at solution surface by intense continuous-wave laser irradiation," Applied Physics Express 11(8), 085502 (2018).
17. S. Pathak, J. A. Dharmadhikari, A. A. Thamizhavel, D. Mathur, and A. K. Dharmadhikari, "Growth of micro-crystals in solution by in-situ heating via continuous wave infrared laser light and an absorber," Journal of Crystal Growth 433, 43–47 (2016).
18. E. Pechkova, G. Maksimov, E. Parshina, E. Maksimov, N. Kutusov, N. Brazhe, I. Tarasova, S. Fiordoro, and N. Claudio, "Raman spectroscopy of protein crystal nucleation and growth," American Journal of Biochemistry and Biotechnology 10(3), 202–207 (2014).
19. A. Rygula, K. Majzner, K. M. Marzec, A. Kaczor, M. Pilarczyk, and M. Baranska, "Raman spectroscopy of proteins: A review," Journal of Raman Spectroscopy 44(8), 1061–1076 (2013).
20. A. V. Frontzek, L. Paccou, Y. Guinet, and A. Hédoux, "Study of the phase transition in lysozyme crystals by Raman spectroscopy," Biochimica et Biophysica Acta (BBA)-General Subjects 1860(2), 412–423 (2016).
21. V. Kocherbitov, J. Latynis, A. Misiuì, J. Barauskas, and G. Niaura, "Hydration of lysozyme studied by Raman spectroscopy," The Journal of Physical Chemistry B 117(17), 4981–4992 (2013).
22. G. Anderle, R. Mendelsohn, "Fourier Transform-Infrared Studies of the Amide III Spectral Region," Biophysical Journal 52(1), 69–74 (1987).
23. B. R. Silver, V. Fülöp, and P. R. Unwin, "Protein crystallization at oil / water interfaces," New Journal of Chemistry 35(3), 602–606 (2011).
24. R. Silver, J. M. A. Grime, New Approaches to Protein Crystallization, Ph.D. Thesis, University of Warwick (2013).

25. Y.-S. Jun, D. Kim, and C. W. Neil, "Heterogeneous Nucleation and Growth of Nanoparticles at Environmental Interfaces," Accounts of Chemical Research 49(9), 1681–1690 (2016).
26. J. R. Hunter, P. K. Kilpatrick, and R. G. Carbonell, "Lysozyme Adsorption at the Air / Water Interface," Journal of Colloid and Interface Science 137(2), 462–482 (1990).
27. C. J. J. Gerard, G. Ferry, L. M. Vuillard, J. A. Boutin, N. Ferte, R. Grossier, N. Candoni, and S. Veesler, "A Chemical Library to Screen Protein and Protein–Ligand Crystallization Using a Versatile Microfluidic Platform," Crystal Growth & Design 18(9), 5130–5137 (2018).
28. D. Tsekova, S. Dimitrova, and C. N. Nanev, "Heterogeneous nucleation (and adhesion) of lysozyme crystals," Journal of Crystal Growth 196(2–4), 226–233 (1999).
29. E. Pechkova, C. Nicolini, "Accelerated protein crystal growth by protein thin film template," Journal of Crystal Growth 231(4), 599–602 (2001).
30. T. Yamazaki, Y. Kimura, P. G. Vekilov, E. Furukawa, M. Shirai, H. Matsumoto, A. E. S. V. Driessche, and K. Tsukamoto, "Two types of amorphous protein particles facilitate crystal nucleation," Proceedings of the National Academy of Sciences 114(9), 2154–2159 (2017).
31. E. Saridakis, S. Khurshid, L. Govada, Q. Phan, D. Hawkins, G. V Crichlow, E. Lolis, S. M. Reddy s, and N. E. Chayen, "Protein crystallization facilitated by molecularly imprinted polymers," Proceedings of the National Academy of Sciences 108(27), 11081–11086 (2011).
32. F. Artusio, R. Pisano, "Surface-induced crystallization of pharmaceuticals and biopharmaceuticals : a review," International Journal of Pharmaceutics 547(1–2), 190–280 (2018).
33. X. Lin, S. Park, D. Choi, J. Heo, and J. Hong, "Mechanically durable superhydrophobic PDMS-candle soot composite coatings with high biocompatibility," Journal of Industrial and Engineering Chemistry 74, 79–85 (2019).
34. B. N. Sahoo, S. Nanda, J. A. Kozinski, and S. K. Mitra, "PDMS/camphor soot composite coating: towards a self-healing and a self-cleaning superhydrophobic surface," RSC Advances 7(25), 15027–15040 (2017).
35. E. Saridakis, N. E. Chayen, "Towards a 'universal' nucleant for protein crystallization," Trends in Biotechnology 27(2), 99–106 (2009).
36. C. N. Nanev, E. Saridakis, and N. E. Chayen, "Protein crystal nucleation in pores," Scientific Reports 7, 35821 (2017).
37. M. A. Hough, "Challenges and solutions for the analysis of in situ, in crystallo micro-spectrophotometric data," Acta Crystallographica Section D: Biological Crystallography 71, 27–35 (2015).
38. G. Gouadec, P. Colomban, "Raman Spectroscopy of nanomaterials: How spectra relate to disorder, particle size and mechanical properties," Progress in Crystal Growth and Characterization of Materials 53(1), 1–56 (2007).
39. N. Kuhar, S. Sil, T. Verma, and S. Umapathy, "Challenges in application of Raman spectroscopy to biology and materials," RSC Advances 8(46), 25888–25908 (2018).
40. N. A. Nevskaya, Y. N. Chirgadze, "Infrared spectra and resonance interactions of amide-I and II vibrations of α-helix," Biopolymers: Original Research on Biomolecules 15(4), 637–648 (1976).
41. A. C. S. Talari, Z. Movasaghi, S. Rehman, and I. U. Rehman, "Raman spectroscopy of biological tissues," Applied Spectroscopy Reviews 50(1), 46–111 (2015).
42. C. Camerlingo, M. Lisitskiy, M. Lepore, M. Portaccio, D. Montorio, S. D. Prete, and G. Cennamo, "Characterization of human tear fluid by means of surface-enhanced raman spectroscopy," Sensors 19(5), 1177 (2019).
43. N. S. Myshakina, Z. Ahmed, and S. A. Asher, "Dependence of Amide Vibrations on Hydrogen Bonding," Journal of Physical Chemistry B 112(38), 11873–11877 (2008).
44. C. Betzel, G. P. Pal, and W. Saenger, "Three-dimensional structure of proteinase K at 0.15-nm resolution," European Journal of Biochemistry 178(1), 155–171 (1988).
45. B. Xu, N. D. Chasteen, "Iron oxidation chemistry in ferritin. Increasing Fe/O2 stoichiometry during core formation," Journal of Biological Chemistry 266(30), 19965–19970 (1991).
46. K. D. Welch, M. E. Van Eden, and S. D. Aust, "Modification of ferritin during iron loading," Free Radical Biology and Medicine 31(8), 999–1006 (2001).
47. A. M. Koorts, M. Viljoen, "Ferritin and ferritin isoforms I : Structure – function relationships , synthesis , degradation and secretion," Archives of Physiology and Biochemistry 1(113), 30–54 (2007).